Solar Wind Outflow and the Chromospheric Magnetic Network

Donald M. Hassler,[1]* Ingolf E. Dammasch,[2] Philippe Lemaire,[3] Pål Brekke,[4] Werner Curdt,[2] Helen E. Mason,[5] Jean-Claude Vial,[3] Klaus Wilhelm[2]

Observations of outflow velocities in coronal holes (regions of open coronal magnetic field) have recently been obtained with the Solar and Heliospheric Observatory (SOHO) spacecraft. Velocity maps of Ne^{7+} from its bright resonance line at 770 angstroms, formed at the base of the corona, show a relationship between outflow velocity and chromospheric magnetic network structure, suggesting that the solar wind is rooted at its base to this structure, emanating from localized regions along boundaries and boundary intersections of magnetic network cells. This apparent relation to the chromospheric magnetic network and the relatively large outflow velocity signatures will improve understanding of the complex structure and dynamics at the base of the corona and the source region of the solar wind.

Understanding the source region and acceleration mechanisms of the solar wind is one of the most challenging problems in solar physics today. The origin of the high-speed solar wind was inferred in the early 1970s (*1*, *2*), and later measured directly with sounding rocket observations (*3*–*5*), to come from open magnetic field regions in the corona called coronal holes. Since then, this view has been widely accepted, although little additional direct observational evidence has been obtained to support these early observations. Understanding the structure of these coronal holes, and the actual source region within the coronal hole responsible for the high-speed streams, is one of the primary objectives of the Solar and Heliospheric Observatory (SOHO) mission (*6*).

We present observations obtained with the Solar Ultraviolet Measurements of Emitted Radiation (SUMER) instrument on SOHO. SUMER is one of 12 instruments on the European Space Agency (ESA)/NASA SOHO spacecraft, which was launched on 2 December 1995. SOHO is in a halo orbit around the Lagrange point L1, about 1.5 million kilometers sunward of Earth with a constant view of the sun. The SUMER instrument (*7*) is a stigmatic ultraviolet (500 to 1610 Å or 50 to 161 nm) grating spectrograph with an off-axis silicon carbide (SiC-CVD) telescope mirror. This mirror can be scanned along two axes to provide pointing and raster images using one of several possible spectrometer entrance slits (typical angular size of slit is 1.0 arc sec by 300 arc sec). Overlapping first- and second-order stigmatic spectra are imaged onto a 1024 pixel by 360 pixel microchannel plate detector (*8*) with a dispersion of 42 to 45 mÅ/pixel (4.2×10^{-3} to 4.5×10^{-3} nm/pixel) in first order and 21 to 22.5 mÅ/pixel in second order. A grating scan mechanism permits selection of the individual bandpass (40 Å in first order and 20 Å in second order), which is imaged onto the detector at a given time. A more complete description of the SUMER instrument can be found in (*7*, *9*, *10*).

Two sets of observations obtained with the SUMER spectrometer provide high-resolution two-dimensional spectroheliograms of a 9 arc min by 5 arc min region in a midlatitude quiet region (22 September 1996 00:40–08:15 UT) and an open magnetic field region of the north polar coronal hole (21 September 1996 00:15–07:30 UT) (Fig. 1). The observational sequences, spectral bandpass, and location of the spectral bandpass on the detector were identical for both sets of observations to minimize any systematic observational or instrumental effects when comparing the two sets of observations. Each spectroheliogram (*11*) contains full spectral information permitting the construction of line-of-sight velocity maps as well as intensity images in emission lines formed over a wide range of temperatures and heights in the solar atmosphere, from the chromosphere (Si II at 1533 Å wavelength, formed at 10^4 K), through the chromosphere-corona transition region (C IV 1548 Å, formed at 10^5 K), to the base of the corona (Ne VIII 770 Å, formed at $10^{5.8}$ K).

The spectral bandpass selected for these studies (Fig. 2A) extends from 1530 to 1550 Å in the first order and 765 to 775 Å in the second order. The overlapping spectral orders permits us to observe many more spectral lines in a given spectral window on the detector and these lines can be used as wavelength and dispersion references to determine the precise wavelength scale of the instrument. The disadvantage is the increased likelihood of weak blends in the overlapping spectral orders which may complicate the analysis by requiring multipeak Gaussian fitting routines. However, the first-order SUMER instrument efficiency (near 1540 Å) is much lower than the second-order efficiency (at 770 Å), thus minimizing this complication. To assess the effect of the numerous weak first-order Si I lines near the second-order Ne VIII 770 Å coronal line, we used a first-order High-Resolution Telescope and Spectrograph (HRTS) spectrum (*12*) from a chromospheric bright point, which produces

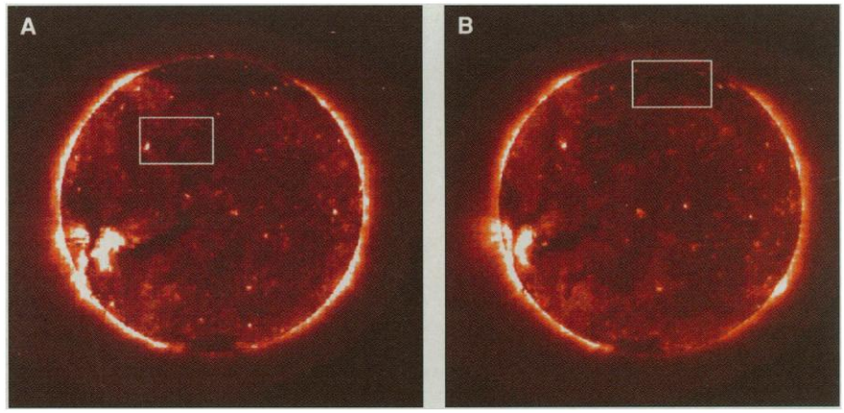

Fig. 1. Outline of the SUMER observations (**A**) in a midlatitude, predominantly closed magnetic field region on 22 September 1996, and (**B**) in the open magnetic field region of the north polar coronal hole on 21 September 1996, superimposed on Fe XII 195 Å images (formed at roughly 1.5 million degrees) taken at the same time with the Extreme Ultraviolet Imaging Telescope (EIT) instrument on SOHO. Bright regions on the disk indicate hot, dense plasma loops. (Images courtesy of the EIT Consortium)

[1]Southwest Research Institute, 1050 Walnut Street, Boulder, CO 80302, USA. [2]Max-Planck-Institut für Aeronomie, D-37191 Katlenburg-Lindau, Germany. [3]Institut d'Astrophysique Spatiale, Unité Mixte CNRS–Université Paris XI, 91405 Orsay, France. [4]Institute of Theoretical Astrophysics, University of Oslo, N-0315 Oslo, Norway. [5]University of Cambridge, Cambridge CB3 9EW, UK.

*To whom correspondence should be addressed. E-mail: hassler@boulder.swri.edu

strong Si I intensities, and scaled it to the SUMER spectrum using common unblended Si I lines in the spectral bandpass (Fig. 2B). We fit the original SUMER profile to a Gaussian distribution, subtracted the scaled first-order HRTS spectrum, and then fit once again the resulting Ne VIII line profile to a Gaussian curve to measure any possible line shifts due to the Si I blends. The result showed a redshift of less than 1 mÅ (0.03 pixels) in the Gaussian line center of the unblended profile with respect to the original SUMER profile, which is within the uncertainty of the measurement (±0.1 to 0.2 pixels). So for these observations, the overlapping first-order Si I blends do not appear to significantly effect the Gaussian fit line centers or wavelengths.

The data were corrected for nonuniformities in the SUMER detector with a "flat field" obtained on 23 September 1996 (to correct for pixel-to-pixel sensitivity variations) and "destretched" (to correct for geometric and thermal distortion) by mapping the data to a grid derived from systematic observations of chromospheric lines. The data were then binned along the slit (y axis) to increase the signal-to-noise ratio and to provide approximately square spatial resolution pixel elements, with an effective pixel size of 3 arc sec by 3 arc sec. The emission lines from the spectrum of each spatial resolution element were fit to a Gaussian profile and linear background using a maximum likelihood technique (*13, 14*), which weighs each data point in the profile according to Poisson statistics (effectively giving more weight to the line center and less weight to the wings in the fitting algorithm). The resulting uncertainties in the Ne VIII 770 Å line, Si II 1533 Å line, and C IV 1548 Å line profile parameters are relatively small, with typical uncertainties in the line center position on the order of ±0.1 to 0.2 pixels (1σ).

The wavelength of the Gaussian center of each Ne VIII 770 Å profile was measured with respect to the Gaussian center position of the overlapping Si II 1533.432 Å profile for that spatial resolution element. Previous rocket observations (*15, 16*) of the wavelength of the chromospheric Si II 1533 Å line with respect to an absolute in-flight wavelength calibration lamp have shown that the wavelength of the solar line agrees with the laboratory rest wavelength of 1533.432 Å to within ±1 to 2 km/s, making this solar chromospheric line a reliable wavelength and velocity reference. The spectrometer wavelength dispersion scale relating the observed wavelength of the Ne VIII line to the Si II line was determined by fitting the Gaussian center position of eight weak nearby first-order Si I lines to a polynomial fit. Each of the wavelengths of these Si I lines agreed with this dispersion curve to within 1 to 2 km/s.

Ne VIII outflow velocities. An accurate determination of the absolute Ne^{7+} Doppler velocities requires both a precise measurement of the Ne VIII 770 Å solar wavelength and an accurate measurement of the laboratory rest wavelength. The Ne VIII solar wavelength discussed here was measured with respect to the overlapping Si II 1533.432 Å line, using the wavelength dispersion curve determined from the nearby Si I lines. The most recent determinations of the Ne VIII 770 Å rest wavelength measured in the laboratory were provided by Bockasten *et al.* (*17*) and Fawcett *et al.* (*18*), both from observations made in the early 1960s. However, the laboratory measurement of highly ionized ions, such as Ne^{7+}, is very difficult, and it has recently been suggested that a more accurate determination can be made from solar observations by making various assumptions about the observations and the solar conditions in which the line is formed (*19, 20*). Although the wavelength precision of current solar observations of many highly ionized ions presently exceeds the accuracy in which the laboratory rest wavelengths have been determined (*19, 21*), the accuracy of these solar rest wavelengths still depends critically on these assumptions.

The spatially averaged Ne VIII wavelength for the observations discussed here was 770.411 ± 0.005 Å for the polar region and 770.419 ± 0.005 Å for the midlatitude region (Fig. 3). Using the laboratory rest wavelengths published by Bockasten *et al.* (*17*) of 770.409 ± 0.005 Å, we find that the observations from the midlatitude region are systematically redshifted (*22*) by 4 to 5 ± 2 km/s. The observations from the polar region tend to be less redshifted, approaching zero redshift at the edge of the polar crown, and then slightly blueshifted (on average) inside the polar coronal hole, consistent with earlier observations (*23*). Using the more recent solar "rest" wavelengths for Ne VIII determined by Dammasch *et al.* (*19*) of 770.428 ± 0.003 Å, we find that the Ne VIII Doppler velocities are, on average, at rest or slightly blueshifted throughout the midlatitude "quiet sun" region, with the line-of-sight velocities inside the coronal hole approaching 5 to 6 km/s toward the blue, suggesting significant outflowing material. In both cases, we see that the observations from the polar region are significantly blueshifted with respect to those from the midlatitude region, indicative of the coronal outflows associated with the fast solar wind.

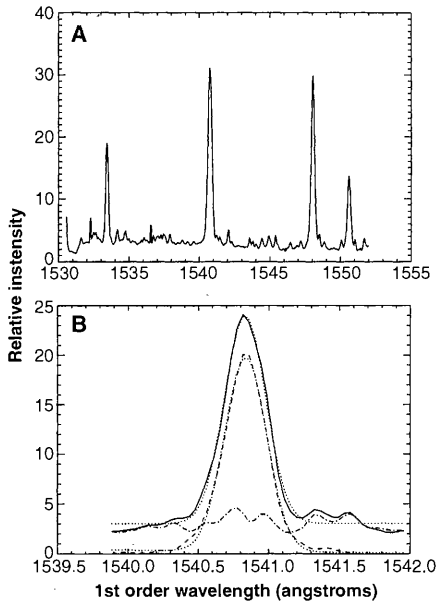

Fig. 2. (**A**) Sample SUMER spectrum showing the 20 Å bandpass used for these observations. The strong second-order line of Ne VIII 770 Å, and the first-order lines of C IV 1548 Å and Si II 1533 Å span a wide range of temperatures and heights in the solar atmosphere. (**B**) SUMER spectrum of the Ne VIII 770 Å line (upper Gaussian curve) superposed with a HRTS first-order spectrum (dot-dashed line) showing the contribution of the small Si I blends. The lower Gaussian curve (dashed line) shows the residual second-order Ne VIII 770 Å profile after the scaled, first-order HRTS spectrum has been subtracted. The dotted lines superimposed on the Gaussian curves show the fits to both Ne VIII profiles (before and after subtracting the contribution of the Si I blends).

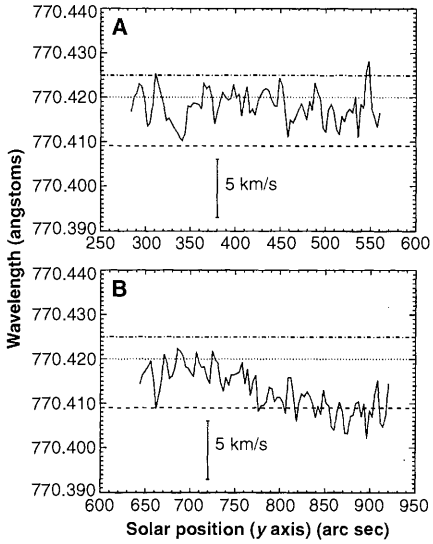

Fig. 3. Observed Ne VIII 770 Å wavelengths of a strip 2 arc min in width near the central meridian as a function of solar position along the north-south axis, illustrating the latitudinal dependence of the Ne VIII velocity structure. These wavelengths are measured with respect to Si II 1533 Å which is assumed to be at rest (±1 to 2 km/s). The dashed line and dotted line represent the "zero velocity" reference wavelength measured in the laboratory by Bockasten *et al.* (*17*) and Fawcett (*18*), respectively. The dot-dashed line represents the "zero velocity" reference wavelength determined from off-limb solar observations (*19, 20*). Observations in (**A**) are from the midlatitude closed magnetic region (22 September 1996) and (**B**) are from the primarily open magnetic field region of the north polar coronal hole (21 September 1996).

Ne VIII velocities and chromospheric network structure. More insight into these outflow velocities and their relationship to atmospheric structures on the sun is gained by studying the full, two-dimensional, co-spatial, co-temporal spectroheliograms from layers in the atmosphere representative of the chromospheric magnetic network (Si II 1533 Å), the chromosphere-corona transition region (C IV 1548 Å), and the corona (Ne VIII 770 Å, formed at the temperature of formation appropriate for coronal holes). Because observations from SOHO have shown that the structure of the chromospheric magnetic network is strongly correlated with chromospheric emission line intensity (*24–26*), we determine the network boundaries for these observations by tracing the outline of the Si II 1533 Å line intensity along the bright network cells (Fig. 4), using visual pattern recognition. Analysis of the C IV transition region observations has also been performed (*27*), revealing strong network structure downflows, similar to previous HRTS observations (*28*) and other SOHO observations (*29, 30*). Superposing the chromospheric network boundaries, determined from the Si II 1533 Å intensity images, on each set of coronal Ne VIII 770 Å intensity images (Fig. 5) shows much less network structure. Note that the bright regions or bright points in the Si II images (Fig. 4) do not necessarily correlate with the coronal bright points or regions, although in each case they tend to occur on the chromospheric network boundaries.

However, superimposing the same chromospheric network boundaries on the coronal Ne VIII velocity images (Fig. 6) reveals a much stronger correlation. In this case, the coronal velocity field is correlated with the chromospheric magnetic network structure below. Blueshifts, or outflows, tend to occur predominantly on network boundaries, with the largest blueshifts (outflows) occurring at the intersection of network boundaries.

In the polar coronal hole observations (Fig. 6B), the blueshifts appear sharp (bright) along the network boundaries and more diffuse outside of the boundaries, which is consistent with a "funnel-like" expansion of the open magnetic field lines originating along the network boundaries (*31–34*). It can also be seen that blueshifts do still occur in the midlatitude region (Fig. 6A), at the intersection of network boundaries, but that the majority of the area, particularly in the cell interiors, is either at rest or redshifted, depending on the Ne VIII rest wavelength reference.

The magnitudes of the line-of-sight Doppler shifts along the network boundaries in the polar coronal hole between 800 and 875 arc sec north of the equator (56° to 65°N solar latitude) are 3 to 6 km/s toward shorter wavelengths. These line-of-sight Doppler shifts correspond to radial outflow velocities of 5 to 12 km/s depending on the location of the observed Doppler shift. Velocities at the intersection of the network boundaries can be greater than the velocities along the network boundary itself, with radial velocities as high as 10 to 20 km/s.

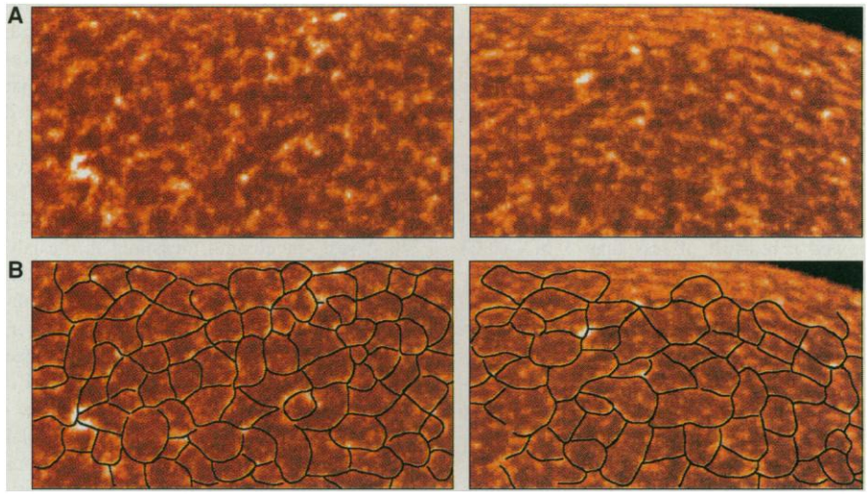

Fig. 4. (**A**) SUMER chromospheric Si II 1533 Å images from a midlatitude region (left) and the north polar region (right). (The location of these 540 × 300 arc sec^2 regions on the solar disk is shown in Fig. 1.) (**B**) The chromospheric network structure, determined by tracing the Si II intensity using visual pattern recognition, is superposed on the lower set of images. White and bright yellow indicate hotter, denser plasma loops along the magnetic network boundaries.

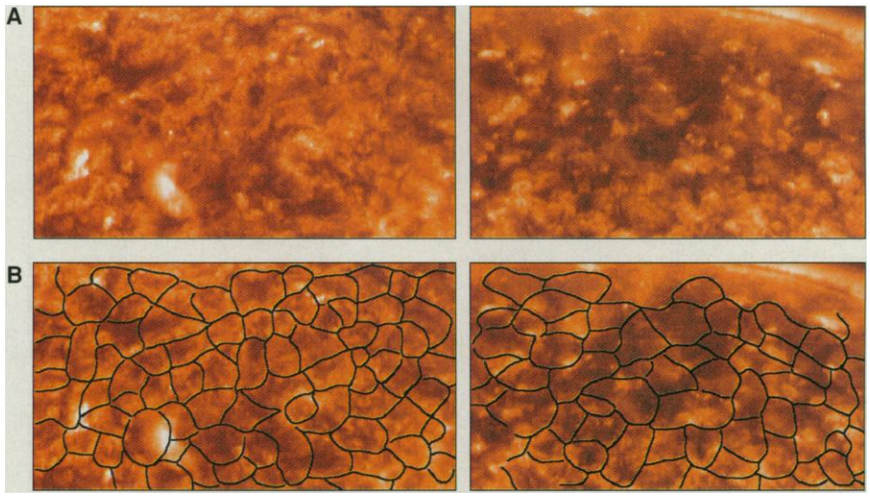

Fig. 5. SUMER Ne VIII 770 Å intensity images from the same region as the Si II images (Fig. 4), with the midlatitude region on the left and the polar region on the right. The chromospheric network is superposed on the lower set of images for comparison with the Si II intensity images in Fig. 4 and the Ne VIII velocity images in Fig. 6.

Discussion. There does not appear to be any exceptional Doppler velocity signature (greater than other regions inside the coronal hole) associated with two polar plumes which are visible against the disk in the north polar coronal hole (upper left region in the right panels of Figs. 5 and 6). The plumes appear wide (≈30 arc sec) and diffuse in Ne VIII (Fig. 5B), with the base of both plumes originating at the intersection of the network boundary. The base of the plumes does not appear any brighter than the rest of the plume in Ne VIII, but does appear to correspond to two chromospheric (Si II 1533 Å) bright points (Fig. 4), which are also located at network intersections. The relationship between polar plumes and the high speed solar wind has been discussed (*24, 35, 36*). The lack of any exceptional blueshift (outflow) signature greater than other regions inside the coronal hole suggests that polar plumes do not provide the bulk of the fast solar wind, although they are part of the outflowing material along the network structure which makes up the fast solar wind.

The relationship between outflow velocity and network structure discussed here is in contrast with recent observations of asymme-

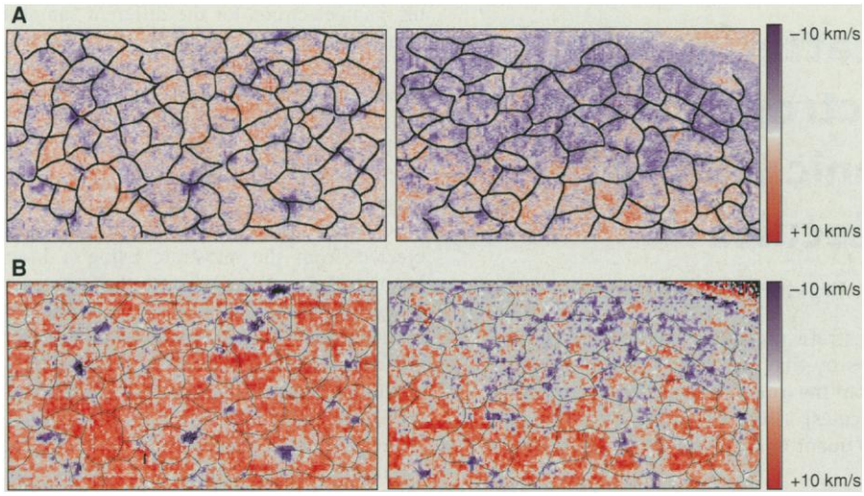

Fig. 6. SUMER Ne VIII 770 Å line-of-sight Doppler velocity images from the midlatitude region (left), and the polar region (right), with the chromospheric network boundaries superimposed. The top images (**A**) were fit using a moments technique on unbinned data and used off-limb solar observations (*19*) to provide the "zero" velocity reference. The bottom two images (**B**) were obtained using Gaussian fitting routines on binned data (to increase the signal-to-noise ratio) and used the "zero velocity" reference wavelength measured in the laboratory by Bockasten *et al.* (*17*). This laboratory rest wavelength is thought to be in error, as suggested by Dammasch *et al.* (*19*) and Peter (*20*), causing zero velocity flows to appear redshifted. However, these images are useful to illustrate the relationship between measured outflow (blue) and magnetic network structure. The panels in this figure are slightly different sizes due to the array size chosen for the binned data prior to performing the Gaussian profile fitting. Blue represents blue shifts or outflows and red represents red shifts or downflows. The velocity scale is roughly ±10 km/s, with the darkest red regions corresponding to roughly 10 km/s redshift and the darkest blue regions corresponding to a 10 km/s blueshift.

tries in the wings of the He I 1083 nm absorption line in a polar coronal hole (*37*). Their results suggest outflows of about 8 km/s found predominantly in the center of supergranular cells, and which are not associated with the bright network structures. However, the formation process of the He I 1083 nm line is complicated (*38*), making it difficult to directly associate wing asymmetries with outflow velocities. Resolution of this discrepancy may lie in a better understanding of the formation of the He I line.

Although our observations suggest that the outflows occur predominantly on network boundaries and at the intersections of network boundaries, there is no clear correlation between Ne^{7+} velocity and Ne VIII intensity (Figs. 5 and 6). The largest Ne^{7+} velocities do not correspond to the brightest structures. One might speculate that the energy funneled up through the network goes into either heating local closed loop structures, such as extreme ultraviolet (EUV) and x-ray bright points, or accelerating material along open magnetic field regions at the boundaries and intersections of the network structure, but not both at the same time. Whether the energy goes into heating the plasma or accelerating it depends critically on the local magnetic field topology.

These strong blueshifts seen along the network boundaries suggest that these regions may be the only place where the magnetic field is open at these heights and temperatures. At midlatitudes, where the fields are typically closed above by high-temperature loops, the only topologically possible solution for open field lines is at the intersections of the network boundaries. In the polar coronal hole, where the large-scale field is open above, the blueshifts become visible along the network boundaries and at the intersections.

In summary, these Ne VIII observations reveal the first two-dimensional coronal images showing velocity structure in a coronal hole, and provide strong evidence that coronal holes are indeed the source of the fast solar wind. The apparent relationship to the chromospheric magnetic network, as well as the relatively large outflow velocity signatures at the intersections of network boundaries at midlatitudes, is a first step in better understanding the complex structure and dynamics at the base of the corona and the source region of the solar wind.

References and Notes

1. A. S. Krieger, A. F. Timothy, E. C. Roelof, *Sol. Phys.* **29**, 505 (1973).
2. J. B. Zirker, Ed., *Coronal Holes and High Speed Wind Streams* (Colorado Associated Univ. Press, Boulder, 1977).
3. G. W. Cushman and W. A. Rense, *Astrophys. J.* **207**, L61 (1976).
4. G. J. Rottman, F. Q. Orrall, J. A. Klimchuk, *ibid.* **260**, 326 (1982).
5. F. Q. Orrall, G. J. Rottman, J. A. Klimchuk, *Astrophys. J. Lett.* **216**, L65 (1983).
6. B. Fleck, V. Domingo, A. I. Poland, Eds., "The SOHO Mission," in *Sol. Phys.* **162**, nos. 1 and 2 (1995).
7. K. Wilhelm *et al.*, *ibid.*, p. 189.
8. O. H. W. Siegmund *et al.*, *Proc. SPIE* **2518**, 344 (1995).
9. K. Wilhelm *et al.*, *Sol. Phys.* **170**, 75 (1997).
10. P. Lemaire *et al.*, *ibid.*, p. 105.
11. The raster sequence used to produce these spectroheliograms consisted of moving the 1 × 300 arc sec slit in roughly 3.0 arc sec steps across a 9 arc min region. This step size, along with an integration time of 150 s per step position provided adequate spatial resolution to resolve fine-scale structures and sufficient signal-to-noise and counting statistics to perform high-resolution spectroscopy.
12. P. Brekke, *Astrophys. J. Suppl. Ser.* **87**, 443 (1993).
13. T. Awaya, *Nucl. Instrum. Methods* **165**, 317 (1979).
14. S. Baker and R. D. Cousins, *ibid.* **221**, 437 (1984).
15. D. M. Hassler, G. J. Rottman, F. Q. Orrall, *Astrophys. J.* **372**, 710 (1991).
16. G. J. Rottman, D. M. Hassler, M. D. Jones, F. Q. Orrall, *ibid.* **358**, 693 (1990).
17. K. Bockasten, R. Hallin, T. P. Hughes, *Proc. Phys. Soc. London* **81**, 522 (1963).
18. B. C. Fawcett, B. B. Jones, R. Wilson, *ibid.* **78**, 1223 (1961).
19. I. E. Dammasch, K. Wilhelm, W. Curdt, D. M. Hassler, *Astron. Astrophys.*, in press.
20. H. Peter, *Astrophys. J.*, in press.
21. P. Brekke and D. Hassler, in *Workshop on Laboratory and Astronomical High-Resolution Spectra*, Brussels, Belgium, 29 August to 2 September 1994, Astronomical Society of the Pacific (ASP) conference series, A. J. Sauval, R. Blomme, N. Grevesse, Eds. (ASP, San Francisco, CA 1995), vol. 81, pp. 589–594.
22. A "redshift" or Doppler shift toward longer wavelengths indicates an object is moving away from observer. A "blueshift" or Doppler shift toward shorter wavelengths indicates an object is moving toward observer.
23. H. P. Warren, J. T. Mariska, K. Wilhelm, *Astrophys. J. Lett.* **490**, L187 (1997).
24. C. E. DeForest *et al.*, *Sol. Phys.* **175**, 393 (1997).
25. Z. Frank, T. Tarbell, J. Covington, *EOS (Spring Suppl.)* **79**, S254 (1998).
26. J. Covington, T. Tarbell, P. Brekke, A. Fludra, M. Ryutova, *ibid.*, p. S265.
27. I. E. Dammasch, D. M. Hassler, W. Curdt, K. Wilhelm, *Proceedings of the SOHO 7 Workshop*, in press.
28. K. Dere, *Astrophys. J.* **305**, 947 (1986).
29. P. Brekke, D. M. Hassler, K. Wilhelm, *Sol. Phys.* **175**, 349 (1997).
30. J. Chae, H. S. Yun, A. I. Poland, *Astrophys. J.* **480**, 817 (1997).
31. A. H. Gabriel, *Philos. Trans. R. Soc. London Ser. A* **281**, 339 (1976).
32. ———, *Proc. IAU Colloq.* **36**, 375 (1977).
33. J. F. Dowdy, D. Rabin, R. L. Moore, *Sol. Phys.* **105**, 35 (1986).
34. E. Marsch and C.-Y. Tu, *ibid.* **176**, 87 (1997).
35. D. M. Hassler, K. Wilhelm, P. Lemaire, U. Schühle, *ibid.* **175**, 375 (1997).
36. K. Wilhelm *et al.*, *Astrophys. J.* **500**, 1023 (1998).
37. A. K. Dupree, M. J. Penn, H. P. Jones, *Astrophys. J. Lett.* **467**, L121 (1996).
38. V. Andretta and H. P. Jones, *Astrophys. J.* **489**, 375 (1997).

39. We give thanks to and acknowledge the essential and untiring help of N. Morisset of the SUMER team for solving all of the operations and software problems and system management bugs with enthusiasm and good humor. SOHO is a project of international cooperation between ESA and NASA. EIT images are courtesy of the SOHO/EIT consortium. The SUMER project is financially supported by DLR, CNES, NASA, and the ESA PRODEX program (Swiss Contribution). A portion of the work of D.M.H. has been supported by NASA under grant NAG 5-6027 to Southwest Research Institute and by CNRS through the "poste rouge" visiting scientist program. H.E.M. acknowledges the financial support of Particle Physics and Astronomy Research Council.

13 August 1998; accepted 18 December 1998